Vibration Analysis of Composite Turbopropellers Using a Nonlinear Beam-Type Finite-Element Approach

J. B. Kosmatka* and P. P. Friedmann†
University of California, Los Angeles, California

An analytical model for determining the free vibration characteristics of advanced composite turbopropellers (prop-fans) is presented. The blade is modeled using a number of straight beam-type finite elements, where the elastic axis of each element is a piecewise straight representation of the curved line of shear centers of the swept blade. The finite-element model is obtained from Hamilton's principle with allowances for: generally anisotropic material behavior, arbitrary cross-sectional properties, large pretwist angles, out-of-plane cross-section warping, and geometrically nonlinear behavior based upon moderate deflection theory. The natural frequencies and mode shapes of the rotating blade are calculated assuming linear perturbations about the nonlinear static equilibrium position of the blade. This model is sufficiently general to analyze other advanced composite aerospace structures. Numerical results are presented to illustrate the versatility of the method by applying it to 1) a conventional propeller (TRW-Hartzell 101/16) and 2) a highly swept and pretwisted isotropic turbopropeller (NASA SR-3). Excellent agreement with experimental test results is obtained for the lower modes of both the conventional propeller and the advanced turbopropeller.

Nomenclature

C_{ij} = material elastic moduli ($i,j = 1-6$)
$\hat{e}_x,\hat{e}_y,\hat{e}_z$ = orthonormal triad of beam element
$\hat{e}_x,\hat{e}_\eta,\hat{e}_\zeta$ = curvilinear coordinate axes of beam element
$\hat{e}_x',\hat{e}_\eta',\hat{e}_\zeta'$ = curvilinear coordinate axes of beam element after deformation
$\{F^T\}$ = applied load and centrifugal force array
$\hat{g}_x,\hat{g}_\eta,\hat{g}_\zeta$ = base vectors of undeformed beam
$\hat{G}_x,\hat{G}_\eta,\hat{G}_\zeta$ = base vectors of deformed beam
h_i,h_j,h_k = translational offsets of element from spin axis (Fig. 3)
$\hat{i},\hat{j},\hat{k}$ = blade-fixed coordinate system (Figs. 2 and 3)
$\hat{i}_0,\hat{j}_0,\hat{k}_0$ = hub-fixed coordinate system (Fig. 2)
$[J^{NL}]$ = self-adjoint nonlinear Jacobian matrix
$[K^T],[K^{NL}]$ = linear and nonlinear stiffness matrices due to elastic and centrifugal forces
$m, m\eta_m, m\zeta_m$ = mass weighted area, first moments, and
$Im_{\eta\eta}, Im_{\zeta\zeta}, Im_{\eta\zeta}$ second moments of the beam cross section
$[M]$, $[M^c]$ = mass and gyroscopic matrices
p_x,p_y,p_z = distributed forces that act along the line of shear centers in $\hat{e}_x,\hat{e}_y,\hat{e}_z$, respectively
$\{q\}$ = nodal displacement array
Q_{ij}' = reduced material stiffness properties ($i,j = 1,5,6$)
$\hat{r}_0$ = position vector of a point on the deformed blade
$\hat{r}$ = position vector from beam element origin to a point on undeformed beam element
$\hat{R}$ = position vector from beam element origin to a point on deformed beam element
t = time
T = kinetic energy
u,v,w = displacement components in $\hat{e}_x,\hat{e}_y,\hat{e}_z$, respectively
u_c,v_c,w_c = displacement components in $\hat{e}_x,\hat{e}_\eta,\hat{e}_\zeta$, respectively
U = strain energy
$\hat{V}$ = velocity vector of a point on rotating blade
W_e = work of nonconservative forces
x,η,ζ = curvilinear coordinate system of beam element
β = pretwist angle of beam
β_p,β_s,β_c = blade pitch, sweep, and precone angles, respectively
β_i,β_j,β_k = beam element to blade system orientation angles (Fig. 3)
$\epsilon_{xx},\epsilon_{\eta\eta},\epsilon_{\zeta\zeta}$, $\gamma_{x\eta},\gamma_{x\zeta},\gamma_{\eta\zeta}$ = strain components
κ_η,κ_ζ = deformed curvatures of the beam
ρ = mass density
$\sigma_{xx},\sigma_{\eta\eta},\sigma_{\zeta\zeta}$, $\sigma_{x\eta},\sigma_{x\zeta},\sigma_{\eta\zeta}$ = strain components
τ_0 = initial beam pretwist ($=\beta_{,x}$)
τ,τ' = deformed and elastic twist of beam, respectively
ϕ = elastic twist angle of beam element
ψ = cross-section warping function
Ω = rotational speed
$()_{,x}()_{,\eta}()_{,\zeta}$ = derivatives with respect to x, η, and ζ, respectively
$\delta()$ = variation of ()
$(\dot{})$ = derivative with respect to time t

Received Oct. 5, 1987; revision received Nov. 23, 1988.

This paper is dedicated to the memory of Dr. Kris Kaza, whose recent death interrupted an outstanding research activity in turboprop aeroelasticity.

*Currently Assistant Professor, Mechanical Engineering Department, Virginia Polytechnic Institute and State University. Member AIAA.

†Professor and Chairman, Mechanical, Aerospace, and Nuclear Engineering Department. Associate Fellow AIAA.

Introduction

A RENEWED interest in propeller-driven aircraft has been recently generated by the potential for significant improvements in fuel efficiency demonstrated in studies sponsored by NASA.[1] These results have shown a significant decrease in fuel consumption (15–30%) for advanced turbo-

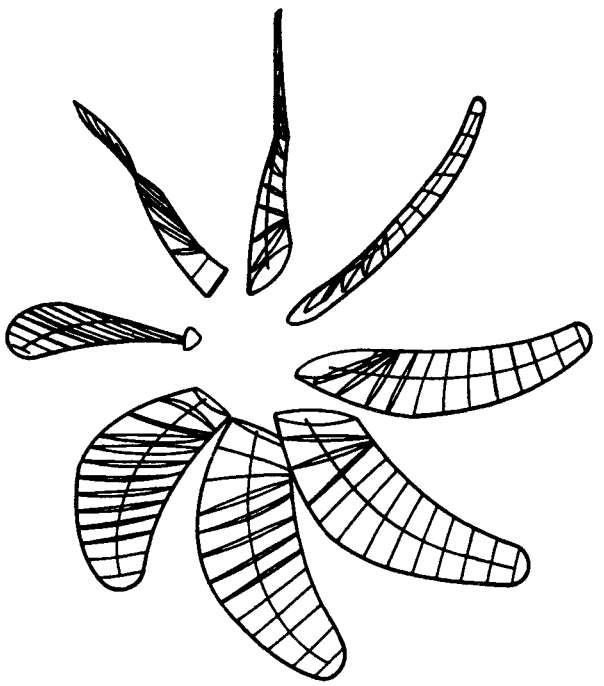

Fig. 1 Advanced turbopropeller showing line of shear centers and finite-element model.

propeller-powered aircraft when compared to conventional turbofan engines. Current design of advanced turbopropeller blades (prop-fans) incorporate a large amount of sweep (up to 60 deg) combined with very thin cross section (3% thickness to chord ratio at blade tip), which can produce large bending and twisting deformations and complex vibratory characteristics. Composite construction is envisioned for such designs as a necessary means to control the deformation and vibration levels and further reduce fuel consumption, noise levels, and manufacturing costs. The use of composite materials could be the key to the successful design of the advanced turboprop by utilizing structural tailoring to generate optimum blade characteristics.[2] Such optimized blades can only be designed by using an accurate mathematical model for a curved blade that can represent the general anisotropic nature of advanced composite materials.

Much of the published research has emphasized the use of a beam-type model. The majority of this work has been in the area of straight isotropic pretwisted helicopter rotors, where it has been recognized that a geometrically nonlinear theory[3-5] and out-of-plane cross-section warping[6-8] are required to correctly model the coupling of the centrifugal and elastic forces. Beam theories have also been developed for analyzing a curved (swept) isotropic blade, where the curvature is defined in a single plane (for example, Ref. 9). These theories, which require that the undeformed elastic axis and the initial curvature distribution of the blade be known, contain complex expressions for the coupling between the elastic displacements and the blade curvatures. The extension of these two theories to represent a curved (general space curve) anisotropic blade would lead to an algebraically intractable model that is not as versatile as a finite-element-based approach.

Recently, three studies aimed at analyzing thin-walled composite helicopter blades using finite-element-based models have become available.[10-12] These studies, which include out-of-plane warping, are limited to single-cell cross sections. Hong and Chopra[10] developed a composite model by extending an earlier isotropic model[3] to include a laminated rectangular box cross section. Bauchau and Hong[11] derived a nonlinear anisotropic model based upon an isoparametric formulation that includes shear deformations and arbitrarily large rotations. The out-of-plane warping function is included using a

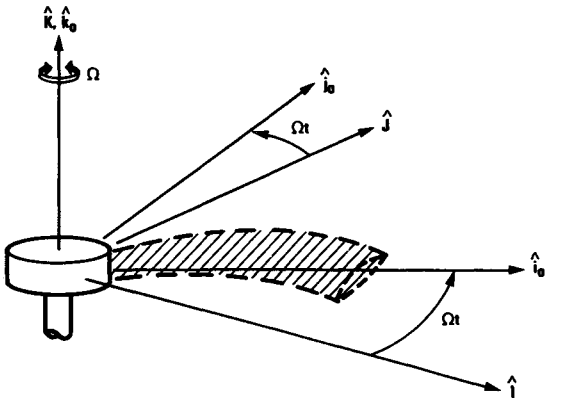

Fig. 2 Hub-fixed and blade-fixed coordinate systems.

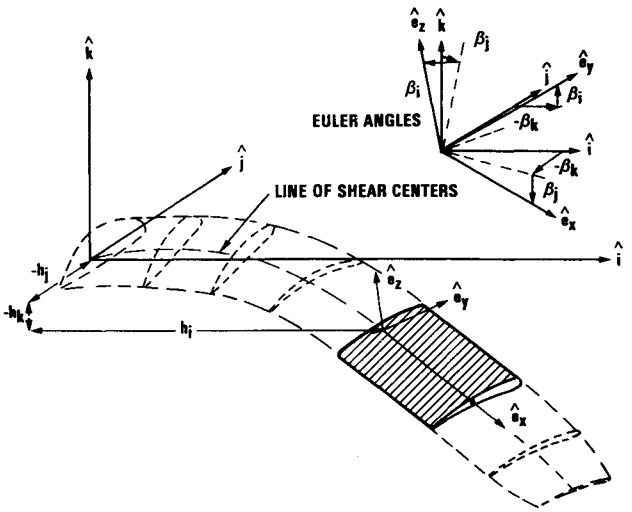

Fig. 3 Blade-fixed and beam element coordinate systems.

partial set of eigenwarping modes that are determined by a separate analysis.[13] Finally, Stemple and Lee[12] developed a blade model that uses isoparametric beam elements to determine the elastic displacements along with a three-dimensional solid-element model for determining the cross-section warping.

The objective of this paper is to develop an analytical model for determining the free vibration characteristics of advanced composite turbopropellers. The blade model is defined using straight beam-type finite elements, where the elastic axis of each element represents a piecewise straight approximation to the curved line of shear centers of the swept blade (Fig. 1). The straight beam-type finite elements are developed using Hamilton's principle. The nonlinear strain-displacement relations are derived assuming moderate deflection theory (small strains and finite rotations) with allowances for out-of-plane warping. The constitutive relations of a generally anisotropic material are used, where the stresses within the cross section and shear deformation effects are neglected. A set of section constants (Appendix), which contain the material and warping couplings, are identified. These section constants along with the warping distribution and shear center are determined by a separate finite-element analysis for a general-shaped cross section composed of either isotropic,[14] multiple monoclinic,[15] or multiple generally anisotropic materials.[16]

Numerical results are presented to illustrate the versatility of the method of applying it to a conventional propeller (TRW/Hartzell 101/16) and to an advanced turbopropeller (NASA SR-3). A more detailed development of the model along with additional numerical examples can be found in Ref. 16.

This model is sufficiently general so as to enable one to analyze other straight or swept advanced-composite aerospace structures (helicopter rotors, propellers, satellite appendages, tilt-rotors, and wind-turbine blades). Such a general model has not been available prior to this study, and it is expected to be valuable for designers and analysts.

Formulation of the Blade Model

The advanced composite turbopropeller is assumed to rotate with a constant angular velocity Ω, and the effects of pitch, precone, and sweep are accounted for (Fig. 2). The blade is divided into a series of subregions modeled by straight anisotropic beam-type finite elements that represent a piecewise approximation to the general curved line of shear centers of the blade (Fig. 3). Each finite element is derived using a curvilinear coordinate system that rotates with the beam pretwist to account for large pretwist-elastic displacement coupling effects (Fig. 4). Several coordinate systems are required to fully describe the geometry and the elastic motion of the blade.

Blade Coordinate Systems and Geometric Preliminaries

A hub-fixed system $(\hat{i}_0,\hat{j}_0,\hat{k}_0)$ and a blade-fixed system $(\hat{i},\hat{j},\hat{k})$ are used to orient the blade relative to the hub, where the hub-fixed system rotates with a constant angular speed $\Omega\hat{k}_0$. Allowance for a general blade setting (sweep, precone, or pitch) is made using an Euler angle transformation between the two coordinate systems (Fig. 2).

An orthonormal triad $(\hat{e}_x,\hat{e}_y,\hat{e}_z)$ is used to locate each beam finite element relative to $\hat{i},\hat{j},\hat{k}$ with three translational offsets (h_i,h_j,h_k) and three orientation angles $(\beta_i,\beta_j,\beta_k)$ (Fig. 3). The vector $\hat{e}_x$ is aligned with the beam element elastic axis and is tangent to the curved line of shear centers. The vectors $\hat{e}_y$ and $\hat{e}_z$ are defined within the element cross section.

Large blade pretwist angle effects are properly accounted for by deriving the beam element strain-displacement relations in the $(\hat{e}_x,\hat{e}_\eta,\hat{e}_\zeta)$ triad, which rotates with the beam pretwist (Fig. 4). The vectors $\hat{e}_\eta$ and $\hat{e}_\zeta$ are defined parallel to the modulus weighted principle axes of the cross section, and the pretwist $\beta(x)$ is defined as the change in their orientation at any location along the beam element.

A transformation between the two element displacement sets is

$$\begin{Bmatrix} u_c \\ v_c \\ w_c \end{Bmatrix} = \begin{bmatrix} 1 & 0 & 0 \\ 0 & \cos\beta & \sin\beta \\ 0 & -\sin\beta & \cos\beta \end{bmatrix} \begin{Bmatrix} u \\ v \\ w \end{Bmatrix} \tag{1}$$

A final orthonormal triad $(\hat{e}_x',\hat{e}_\eta',\hat{e}_\zeta')$ is required in the derivation of the nonlinear strain-displacement relations. The triad $(\hat{e}_x,\hat{e}_\eta,\hat{e}_\zeta)$, which is defined on the elastic axis of the beam before deformation, is carried to $\hat{e}_x',\hat{e}_\eta',\hat{e}_\zeta'$ through rigid-body translations and rigid-body rotations during deformation. The vector $\hat{e}_x'$ is tangent to the deformed elastic axis, and the vectors $\hat{e}_\eta'$ and $\hat{e}_\zeta'$ are defined in the deformed cross section. The deformation of an element dx on the beam elastic axis is described in Fig. 5, where the effects of the rigid-body translation

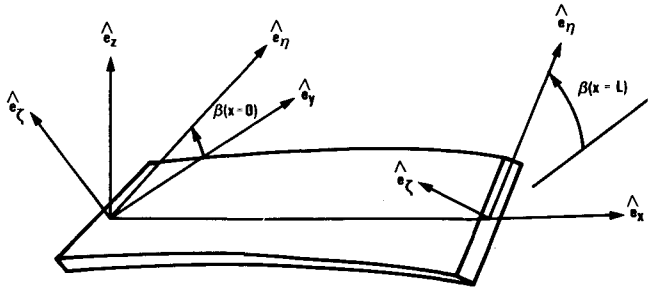

Fig. 4 Element and curvilinear coordinate system of the pretwisted beam element.

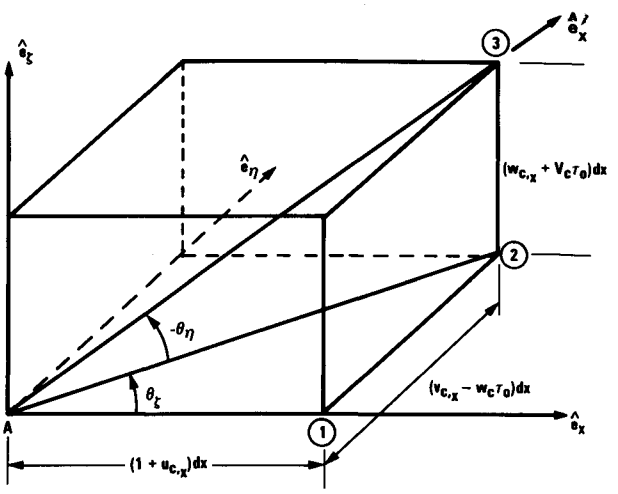

Fig. 5 Curvilinear coordinate system after deformation and orientation angles.

are not shown. Writing the relation between $\hat{e}_x'$ and the curvilinear coordinate system

$$\hat{e}_x' = (1+u_{c,x})\hat{e}_x + (v_{c,x}-w_c\tau_0)\hat{e}_\eta + (w_{c,x}+v_c\tau_0)\hat{e}_\zeta \tag{2}$$

The transformation from the triad $\hat{e}_x,\hat{e}_\eta,\hat{e}_\zeta$ to the set $\hat{e}_x',\hat{e}_\eta',\hat{e}_\zeta'$ is defined using finite orientation angles, where the triad $\hat{e}_x',\hat{e}_\eta',\hat{e}_\zeta'$ is initially aligned with $\hat{e}_x,\hat{e}_\eta,\hat{e}_\zeta$, and the rotations of magnitude θ_ζ, θ_η, and θ_x are performed about $\hat{e}_\zeta'$, $-\hat{e}_\eta'$, and $\hat{e}_x'$, respectively. This sequence was chosen to follow the work of previous authors,[3,4] but other sequences are also possible, and the form of the transformation will differ slightly. An ordering scheme was used to simplify these relations by neglecting the axial strain $(u_{c,x})$ and the squares of the slopes and rotations $(v_{c,x}^2, w_{c,x}^2, \phi^2)$ with respect to unity. This scheme is consistent with a moderate deflection theory (small strains and moderate rotations). The final form of the transformation is defined

$$\begin{Bmatrix} \hat{e}_x' \\ \hat{e}_\eta' \\ \hat{e}_\zeta' \end{Bmatrix} = [T_{DC}] \begin{Bmatrix} \hat{e}_x \\ \hat{e}_\eta \\ \hat{e}_\zeta \end{Bmatrix} \tag{3}$$

where $[T_{DC}]$ is expressed as

$$\begin{bmatrix} 1 & (v_{c,x}-w_c\tau_0) & (w_{c,x}+v_c\tau_0) \\ -(v_{c,x}-w_c\tau_0)-\phi(w_{c,x}+v_c\tau_0) & 1 & \phi \\ -(w_{c,x}+v_c\tau_0)+\phi(v_{c,x}-w_c\tau_0) & -\phi-\tau_c & 1 \end{bmatrix}$$

and

$$\tau_0 = (v_{c,x}-w_c\tau_0)(w_{c,x}+v_c\tau_0)$$

A transformation from the set $(\hat{e}_x,\hat{e}_y,\hat{e}_z)$ to the triad $(\hat{e}_x',\hat{e}_\eta',\hat{e}_\zeta')$ in terms of u, v, and w is determined by combining the above relations [Eqs. (1) and (3)]

$$\begin{Bmatrix} \hat{e}_x' \\ \hat{e}_\eta' \\ \hat{e}_\zeta' \end{Bmatrix} = [T_{DE}] \begin{Bmatrix} \hat{e}_x \\ \hat{e}_y \\ \hat{e}_z \end{Bmatrix} \tag{4}$$

where $[T_{DE}]$ is expressed as

$$\begin{bmatrix} 1 & v_{,x} & w_{,x} \\ -v_{,x}\cos(\beta+\phi)-w_{,x}\sin(\beta+\phi) & \cos(\beta+\phi) & \sin(\beta+\phi) \\ v_{,x}\sin(\beta+\phi)-w_{,x}\cos(\beta+\phi) & -\sin(\beta+\phi+\phi') & \cos(\beta+\phi) \end{bmatrix}$$

and

$$\phi' = (v_{,x}\cos\beta + w_{,x}\sin\beta)(w_{,x}\cos\beta - v_{,x}\sin\beta)$$

This transformation is in general agreement with a similarly derived relation[3] except for the second-order twist term ϕ', where differences are due to the definition of the torsional kinematic variable ϕ.

The curvatures and the twist of the deformed beam are calculated from the theory of space curves (e.g., Wempner, Ref. 17, p. 357, Eqs. 8–19) using Eq. (4) along with the ordering scheme.

$$\kappa_\eta = \hat{e}'_\eta \cdot \hat{e}'_{x,x} = v_{,xx}\cos(\beta+\phi) + w_{,xx}\sin(\beta+\phi) \tag{5a}$$

$$\kappa_\zeta = \hat{e}'_\zeta \cdot \hat{e}'_{x,x} = -v_{,xx}\sin(\beta+\phi) + w_{,xx}\cos(\beta+\phi) \tag{5b}$$

$$\tau = \hat{e}'_\zeta \cdot \hat{e}'_{\eta,x} = \tau_0 + \tau' \tag{5c}$$

where

$$\tau' = \phi_{,x} + \{w_{,x}\cos\beta - v_{,x}\sin\beta\}\{v_{,xx}\cos\beta + w_{,xx}\sin\beta\} \tag{5d}$$

and the small-angle assumption is used for ϕ:

$$\begin{aligned}\cos(\beta+\phi) &\simeq \cos\beta - \phi\sin\beta \\ \sin(\beta+\phi) &\simeq \sin\beta + \phi\cos\beta\end{aligned} \tag{5e}$$

The position vector $\hat{r}$ for the undeformed beam is given by

$$\hat{r} = x\hat{e}_x + \eta\hat{e}_\eta + \zeta\hat{e}_\zeta \tag{6}$$

and the corresponding undeformed base vectors $(\hat{g}_x, \hat{g}_\eta, \hat{g}_\zeta)$ are defined by

$$\hat{g}_x = \hat{r}_{,x} = \hat{e}_x - \zeta\tau_0\hat{e}_\eta + \eta\tau_0\hat{e}_\zeta \tag{7a}$$

$$\hat{g}_\eta = \hat{r}_{,\eta} = \hat{e}_\eta \tag{7b}$$

$$\hat{g}_\zeta = \hat{r}_{,\zeta} = \hat{e}_\zeta \tag{7c}$$

Similarly, the position vector $\hat{R}$ for the deformed beam is defined as

$$\hat{R} = \{x + u_c, v_c, w_c\}\begin{Bmatrix}\hat{e}_x\\ \hat{e}_\eta\\ \hat{e}_\zeta\end{Bmatrix} + \{\psi\tau', \eta, \zeta\}\begin{Bmatrix}\hat{e}'_x\\ \hat{e}'_\eta\\ \hat{e}'_\zeta\end{Bmatrix} \tag{8}$$

where the first term is the deformation of a point on the elastic axis, and the second term contains the rigid rotation of the cross section along with the out-of-plane warping of the cross section due to Saint Venant torsion. The base vectors for the deformed beam $(\hat{G}_x, \hat{G}_\eta, \hat{G}_\zeta)$ are defined as

$$\hat{G}_x = \hat{R}_{,x}, \qquad \hat{G}_\eta = \hat{R}_{,\eta}, \qquad \hat{G}_\zeta = \hat{R}_{,\zeta} \tag{9}$$

Strain Components

The strain components are defined in the curvilinear coordinate system of the beam element using the definitions presented by Wempner (Ref. 17, Eqs. 8–15):

$$\epsilon_{xx} = \frac{1}{2}\left\{\frac{\hat{G}_x \cdot \hat{G}_x}{\hat{g}_x \cdot \hat{g}_x} - 1\right\} \tag{10a}$$

$$\epsilon_{\eta\eta} = \frac{1}{2}\left\{\hat{G}_\eta \cdot \hat{G}_\eta - 1\right\} \tag{10b}$$

$$\gamma_{x\eta} = \left\{\frac{\hat{G}_x \cdot \hat{G}_\eta - \hat{g}_x \cdot \hat{g}_\eta}{\sqrt{\hat{g}_x \cdot \hat{g}_x}}\right\} \tag{10c}$$

$$\epsilon_{\zeta\zeta} = \frac{1}{2}\left\{\hat{G}_\zeta \cdot \hat{G}_\zeta - 1\right\} \tag{10d}$$

$$\gamma_{x\zeta} = \left\{\frac{\hat{G}_x \cdot \hat{G}_\zeta - \hat{g}_x \cdot \hat{g}_\zeta}{\sqrt{\hat{g}_x \cdot \hat{g}_x}}\right\} \tag{10e}$$

$$\gamma_{\eta\zeta} = \left\{\hat{G}_\eta \cdot \hat{G}_\zeta\right\} \tag{10f}$$

Substituting Eqs. (7) and (9) into (10) and applying the ordering scheme

$$\begin{aligned}\epsilon_{xx} = {} & u_{,x} + \tfrac{1}{2}(v_{,x})^2 + \tfrac{1}{2}(w_{,x})^2 + (\psi\phi_{,x})_{,x} + \underline{\tfrac{1}{2}(\eta^2+\zeta^2)(\phi_{,x})^2} \\ & - v_{,xx}\left\{\eta\cos(\beta+\phi) - \zeta\sin(\beta+\phi)\right\} \\ & - w_{,xx}\left\{\zeta\cos(\beta+\phi) + \eta\sin(\beta+\phi)\right\}\end{aligned} \tag{11a}$$

$$\gamma_{x\eta} = \tfrac{1}{2}(\psi_{,\eta} - \zeta)\tau' \tag{11b}$$

$$\gamma_{x\zeta} = \tfrac{1}{2}(\psi_{,\zeta} + \eta)\tau' \tag{11c}$$

$$\epsilon_{\eta\eta} \simeq \epsilon_{\zeta\zeta} \simeq \gamma_{\eta\zeta} \simeq 0 \tag{11d–f}$$

where the underlined term is a higher-order effect that should be neglected based upon the present order scheme, but was retained to include important nonlinear tension-torsion coupling effects.[3,7,10]

The axial strain due to cross-section warping $(\psi\phi_{,x})_{,x}$ can be written in an alternate form, since cross-section warping is a function of η and ζ only:

$$(\psi\phi_{,x})_{,x} = \psi\phi_{,xx} + \{\psi_{,\eta}\zeta - \psi_{,\zeta}\eta\}\tau_0\phi_{,x} \tag{12}$$

Constitutive Relations

The constitutive relations are defined based upon two assumptions: 1) the material exhibits generally anisotropic behavior (fully populated material stiffness matrix), so that all possible material coupling effects are properly accounted for, and 2) the stresses within the cross section are set to zero ($\sigma_{\eta\eta} = \sigma_{\zeta\zeta} = \sigma_{\zeta\eta} = 0$). These assumptions will correctly model the overall blade behavior for all isotropic and most composite material configurations, but further development may be required for highly anisotropic definitions (i.e., relaxation of second assumption and including shear deformation effects).

The stress-strain relations for general anisotropic material behavior, including orthotropic materials where the material axes do not align with the coordinate axes, are

$$\begin{Bmatrix}\sigma_{xx}\\ \sigma_{\eta\eta}\\ \sigma_{\zeta\zeta}\\ \sigma_{\eta\zeta}\\ \sigma_{x\zeta}\\ \sigma_{x\eta}\end{Bmatrix} = \begin{bmatrix} C_{11} & C_{12} & C_{13} & C_{14} & C_{15} & C_{16} \\ & C_{22} & C_{23} & C_{24} & C_{25} & C_{26} \\ & & C_{33} & C_{34} & C_{35} & C_{36} \\ & & & C_{44} & C_{45} & C_{46} \\ \text{symmetric} & & & & C_{55} & C_{56} \\ & & & & & C_{66}\end{bmatrix}\begin{Bmatrix}\epsilon_{xx}\\ \epsilon_{\eta\eta}\\ \epsilon_{\zeta\zeta}\\ \gamma_{\eta\zeta}\\ \gamma_{x\zeta}\\ \gamma_{x\eta}\end{Bmatrix} \tag{13}$$

The constitutive relations are obtained by setting the three stresses within the cross section equal to zero and applying back-substitution:

$$\begin{Bmatrix}\sigma_{xx}\\ \sigma_{x\zeta}\\ \sigma_{x\eta}\end{Bmatrix} = \begin{bmatrix} Q'_{11} & Q'_{15} & Q'_{16} \\ Q'_{15} & Q'_{55} & Q'_{56} \\ Q'_{16} & Q'_{56} & Q'_{66}\end{bmatrix}\begin{Bmatrix}\epsilon_{xx}\\ \gamma_{x\zeta}\\ \gamma_{x\eta}\end{Bmatrix} \tag{14}$$

where

$$[Q'] = [C_{bb}] - [C_{bs}][C_{ss}]^{-1}[C_{sb}]$$

$$[C_{bb}] = \begin{bmatrix} C_{11} & C_{15} & C_{16} \\ C_{15} & C_{55} & C_{56} \\ C_{16} & C_{56} & C_{66} \end{bmatrix}, \qquad [C_{ss}] = \begin{bmatrix} C_{22} & C_{23} & C_{24} \\ C_{23} & C_{33} & C_{34} \\ C_{24} & C_{34} & C_{44} \end{bmatrix}$$

$$[C_{bs}] = [C_{sb}]^T = \begin{bmatrix} C_{12} & C_{13} & C_{14} \\ C_{25} & C_{35} & C_{45} \\ C_{26} & C_{36} & C_{46} \end{bmatrix}$$

Hamilton's Principle

The nonlinear equations of motion and the corresponding finite-element matrices are derived for each beam element using Hamilton's principle:

$$\int_{t_1}^{t_2} (\delta U - \delta T - \delta W_e)\, dt = 0 \tag{15}$$

where δU, δT, and δW_e represent the strain energy variation, kinetic energy variation, and virtual work of external forces, respectively.

Strain Energy

The variation of the strain energy for the anisotropic beam element is defined as

$$\delta U = \int_0^L \iint_A \begin{Bmatrix} \delta\epsilon_{xx} \\ \delta\gamma_{x\zeta} \\ \delta\gamma_{x\eta} \end{Bmatrix}^T \begin{bmatrix} Q'_{11} & Q'_{15} & Q'_{16} \\ Q'_{15} & Q'_{55} & Q'_{56} \\ Q'_{16} & Q'_{56} & Q'_{66} \end{bmatrix} \begin{Bmatrix} \epsilon_{xx} \\ \gamma_{x\zeta} \\ \gamma_{x\eta} \end{Bmatrix} d\zeta\, d\eta\, dx \tag{16}$$

where the stresses within the cross section are set to zero ($\sigma_{\eta\eta} = \sigma_{\zeta\zeta} = \sigma_{\eta\zeta} = 0$), and the strains have been previously defined [Eqs. (11a-f)].

Integrating Eq. (16) with respect to η and ζ will yield the strain energy variation in terms of the linear and nonlinear displacements along with three sets of modulus weighted section constants (Appendix, nos. 1-3). These constants are determined by a separate analysis and are dependent upon the cross-section shape and material lay-up, the out-of-plane warping function, and the shear center location.

Analytical models for determining the warping distribution and the shear center location of general cross sections composed of isotropic,[14] multiple monoclinic,[15] or multiple generally anisotropic materials[16] are available. These models are based upon solving Saint Venant's flexure and torsion problems. The model of Ref. 16 uses the principle of minimum potential energy and a finite-element formulation to discretize the nonhomogeneous two-dimensional boundary-value problem and solve for three unknown coupled displacement functions. These unknown functions (two in-plane and one out-of-plane) are required to describe the displacement and stress distribution of anisotropic materials,[18] whereas only one out-of-plane warping function is required for isotropic or monoclinic material behavior.

The first set of section constants (Appendix, no. 1) are the modulus weighted section integrals. The modulus weighted area and the first and second moments are defined as EA, EA_η, EA_ζ, $EI_{\eta\eta}$, $EI_{\zeta\zeta}$ and $EI_{\eta\zeta}$. Second-order constants that exhibit axial-bending-torsion coupling are defined as EAC_0, EAC_1, and EAC_2. The constant EAC_3 is also a second-order term that modifies the nonlinear torsional stiffness.

The modulus weighted warping integrals are defined in Appendix, no. 2. The torsion constant is defined as GJ. The term EAD_0 represents the warping-axial displacement coupling, and EAD_1 is the coupling due to the first derivative of the warping and the axial displacements. The terms EAD_1 and EAD_2 are used to couple the axial strain of section warping with the transverse displacements, whereas EAD_1' and EAD_2' represent the coupling of the first derivative of the axial strain due to section warping with the transverse displacements. The quantities EAD_3, EAD_3', and EAD_5 represent the change of the torsional stiffness of the beam due to section warping and/or varying section properties (i.e., pretwist). The constants EAD_4 and EAD_4' are second-order torsion coupling terms.

The third set of section constants (Appendix, no. 3) are a result of using materials that exhibit anisotropic behavior. The constants EAB_0, EAB_1, and EAB_2 couple the torsion displacement ϕ with the u, v, and w displacements, respectively. The terms EAB_3 and EAB_3' represent the change in the torsion stiffness of the anisotropic beam due to warping and pretwist of the beam, respectively. The constant EAB_4 is a second-order term that couples the linear and nonlinear torsion deflections of the beam. The terms EAB_0, EAB_1, EAB_2, EAB_3, and EAB_4 will reduce to similar constants presented in Ref. 10, when the laminated cross section is defined as a single thin-wall rectangular cell.

For pretwisted beams with uniform cross sections, the constants EAD_0', EAD_1', EAD_2', EAD_3', EAD_4', and EAB_3' can be defined making use of the following substitution [from Eq. (12)]:

$$\psi_{,x} = \{\psi_{,\eta}\zeta - \psi_{,\zeta}\eta\}\tau_0 \tag{17}$$

Kinetic Energy

The kinetic energy of each beam element is defined as

$$T = \frac{1}{2}\int_0^L \iint_A \rho \hat{V} \cdot \hat{V}\, d\eta\, d\zeta\, dx \tag{18}$$

where

$$\hat{V} = \hat{r}_0 + \Omega \hat{k}_0 x \hat{r}_0 \tag{19}$$

and $\hat{r}_0$ is given by

$$\hat{r}_0 = \{h_i\hat{i} + h_j\hat{j} + h_k\hat{k}\} + \hat{R} \tag{20}$$

The variation of the kinetic energy δT is determined by taking the dot product of $\hat{V}$ with $\delta\hat{V}$ integrating by parts with respect to time and, finally, integrating over the cross section. This integration will yield the mass, the first mass moment, and the second mass moment constants of the cross section about the shear center (Appendix, no. 4).

External Work Contributions

The principle of virtual work is used to include the effects of nonconservative distributed loads.

$$\delta W_e = \int_0^L (p_x \delta u + p_y \delta v + p_z \delta w)\, dx \tag{21}$$

Formulation of the Finite-Element Matrices

The finite-element method is a piecewise application of the variational method. The solution procedure is not based on solving the nonlinear differential equations of motion, but minimizing the total dynamic potential of the rotating blade (i.e., apply Hamilton's principle to each subregion or element of the blade).

Writing Hamilton's principle in discretized form

$$\int_{t_1}^{t_2} \sum_{i=1}^{n} (\delta U_i - \delta T_i - \delta W_{ei})\, dt = 0 \tag{22}$$

where n is the total number of finite elements.

The finite-element matrices are generated by substituting cubic Hermite interpolation polynomials for the axial (u) and the transverse deflections (v, w) and a quadratic Hermite polynomial for the torsion (ϕ) displacement. The quadratic polynomial has the capability of modeling the linear variation of

strain along the element length, thus being compatible with the cubic polynomial for transverse deflections. The resulting matrices have 15 nodal parameters: six at each end of the beam element (three deflections, three rotations) and three internal nodes (two axial and one torsion deflection).

Substituting the interpolation polynomials into the discretized form of Hamilton's principle [Eq. (22)], integrating over the length of each beam, and assembling the n elements yield the nonlinear equations of motion:

$$\int_{t_1}^{t_2} \{\delta q\}^T \Big([M]\{\ddot{q}\} + [M^C]\{\dot{q}\} + \Big[[K^T] + [K^{NL}\{q\}] \Big] \{q\} + \{F^T\} \Big) \, dt = 0 \tag{23}$$

These matrices represent a complete set of self-adjoint finite elements (i.e., symmetric linear matrices and nonlinear Jacobian matrix, and skew-symmetric gyroscopic matrix). Individual matrix coefficients are presented in Ref. 16.

The nonlinear equations of motion can be obtained directly from Eq. (23), noting that $\{\delta q\}$ is arbitrary over the time integral:

$$[M]\{\ddot{q}\} + [M^C]\{\dot{q}\} + \Big[[K^T] + [K^{NL}\{q\}] \Big] \{q\} + \{F^T\} = \{0\} \tag{24}$$

Method of Solution

The solution for the free-vibration characteristics of an advanced composite turbopropeller is accomplished in three steps. First, the finite-element blade model is created by 1) determining the line of shear centers, 2) discretizing the line of shear centers into n beam-type subregions ($n+1$ nodes), 3) calculating the section constants of Appendix using cross-section profiles defined at each node and perpendicular to the line of shear centers, and 4) generate and assemble the finite-element matrices. The line of shear centers is determined by an iterative process, where each successive prediction is calculated by fitting a cubic spline through the shear center locations of section profiles that are perpendicular to a previous prediction. Convergence has occurred when two successive predictions are within 10^{-4}.

Second, the nonlinear static equilibrium position of the blade is determined by neglecting the time-dependent terms from Eq. (24) and solving the following nonlinear equations using a Newton-Raphson iteration scheme:

$$\Big[[K^T] + [K^{NL}\{q\}] \Big] \{q\} + \{F^T\} = \{0\} \tag{25}$$

where convergence has occurred when the absolute change of all deformations is less than 10^{-4} for each iteration.

Finally, the free-vibration frequencies are obtained by assuming that the motion is a linear perturbation $\{\Delta q\}$ about the nonlinear static equilibrium position and applying an appropriate eigenvalue routine.[19]

$$[M]\{\Delta\ddot{q}\} + [M^C]\{\Delta\dot{q}\} + \Big[[K^T] + [J^{NL}\{q\}_n] \Big] \{\Delta q\} = \{0\} \tag{26}$$

where products of the perturbations (i.e., $\Delta q_i \Delta q_j = 0$) are neglected.

Results and Discussion

Numerical results are presented for a conventional propeller (TRW/Hartzell 101/16) and an advanced turbopropeller (NASA SR-3). These results include the determination of the nonlinear static equilibrium position and the free-vibration frequencies of the rotating blades, and suitable correlation with experimental test data. The beam-type properties of these isotropic blades (i.e., line of shear centers, section constants, etc.) were determined using blade planform data together with a separate computer program.[20] Many additional numerical examples that were used to verify this analytical blade model are presented in Ref. 16. It is important to note that these results clearly indicate that the piecewise continuous model, based upon straight finite elements, provides an excellent approximation to the curved beam. Because of lack of space, these results cannot be included in this study.

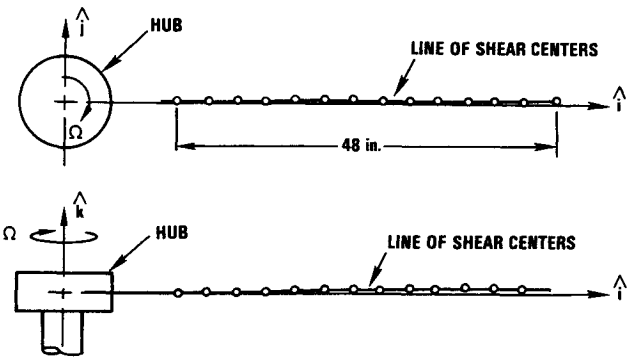

Fig. 6 Finite-element model of TRW/HARTZELL 101/16 propeller.

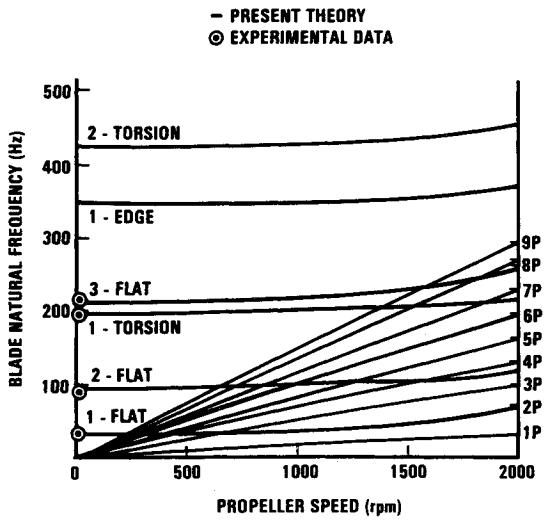

Fig. 7 Test and predicted natural frequencies for the Hartzell 101/16 (Campbell Diagram).

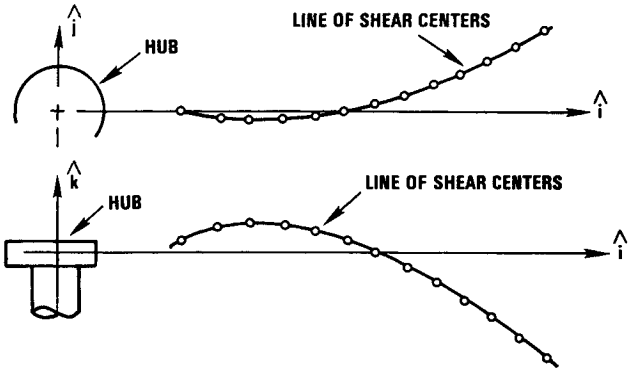

Fig. 8 Finite-element model of NASA SR-3 turbopropeller.

TRW/Hartzell 101/16

The TRW/Hartzell 101/16 is a straight aviation propeller that is 1.22 m (48 in.) long, composed of 2025-T6 aluminum, and highly pretwisted (30 deg). The blade was modeled using

12 beam finite elements that were placed along the line of shear centers (Fig. 6). Photographs of the experimental test setup along with the four lowest vibration mode shapes are presented in Refs. 16 and 21. The blade motion in these lower modes is predominantly uncoupled spanwise bending and torsion with negligible chordwise deformation.

A Campbell diagram is presented in Fig. 7 to show a comparison of the predicted natural frequencies and the experimental results. There is excellent agreement for the first three flatwise bending modes and the first torsion mode, which is a result of having accurate blade properties and negligible chordwise deformation. The increased blade natural frequencies are due to larger centrifugal forces at higher propeller speeds. Experimental data for the rotating blade are not currently available.

NASA SR-3

An advanced turbopropeller (NASA SR-3), which is highly swept (up to 45 deg) and pretwisted (32.5 deg), was also analyzed. The titanium blade was modeled using 12 beam-type finite elements that were defined along the generally curved line of shear center (Figs. 1 and 8). The section profiles undergo rapid changes along the blade length to reduce noise, weight, and centrifugal force. For example, at the blade root the section is relatively thick (20%) with negative camber (3.5%), whereas at the blade tip the section is very thin (3.3%) with positive camber (2.7%).[16,21] In order to obtain accurate results, it was important to include the thickness-wise offsets between the shear center and the mass and area center (i.e., assume nonsymmetric section profiles).

The first four experimentally determined mode shapes (three flatwise bending, one torsion) are predominantly spanwise motion (bending or twisting along the line of shear centers) with negligible chordwise deformation.[16] The higher modes are described as coupled spanwise and chordwise deformation. The current beam-type model, which is based on a one-dimensional theory, has the ability to capture the spanwise motion only. To correctly analyze these higher coupled modes, it is suggested that a two-dimensional shell-type model be used.

A comparison of the predicted natural frequencies and the experimental results for different operating speeds is presented on a Campbell diagram (Fig. 9). For the nonrotating blade ($\Omega = 0$), the experimental results are in agreement with the predicted results for the first four modes. The inclusion of out-of-plane warping (Appendix A, no. 2) is very important for these thin sections because blade pretwist and camber will significantly alter the blade stiffness. The experimental results of the rotating blade (7000 rpm and 8000 rpm) show very good correlation with the finite-element model for the first three modes when the effects of warping are included.

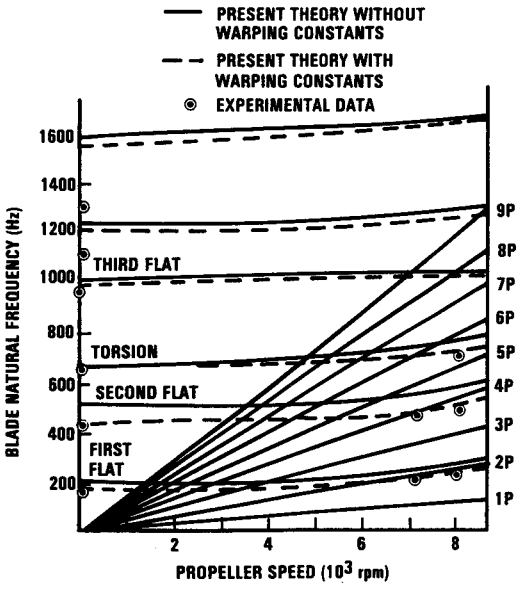

Fig. 9 Test and predicted natural frequencies for the NASA SR-3 turbopropeller (Campbell Diagram).

Conclusions

An analytical model has been developed for determining the free-vibration characteristics of advanced composite turbopropellers. This beam-type finite-element model is sufficiently general so that other types of advanced composite blades such as helicopter blades can also be analyzed. Numerical results have been presented to illustrate the versatility of this model by applying it to a conventional propeller and a highly swept and pretwisted advanced turbopropeller. The following conclusions should only be considered as indicative of trends, since the full effect of geometric coupling (blade sweep and pretwist) and material coupling (composite construction) is unique for each blade configuration.

1) The lower modes and frequencies of advanced composite turbopropellers can be obtained using a nonlinear beam-type finite-element model, where straight elements represent a piecewise continuous approximation of the curved line of shear centers of the blade. The quality of the resulting structural model is strongly dependent upon an accurate determination of the line of shear centers, warping distribution, and section constants (Appendix A).

2) The effect of large blade pretwist angles is properly accounted for by developing the nonlinear strain-displacement relations in a curvilinear coordinate system that rotates with the pretwist.

3) All of the material coupling terms present in composite blades have been identified. These constants were derived assuming generally anisotropic behavior, and stresses within the cross section are negligible.

4) Excellent agreement between the analytical predictions and the experimental results was obtained for the lower modes of an advanced turbopropeller. The inclusion of out-of-plane warping and thickness-wise section offsets (i.e., assume nonsymmetric sections) improved the correlation by altering the coupling stiffness of these thin cambered cross sections.

5) Fair agreement between the analytical predictions and the experimental results was obtained for the higher modes due to the presence of chordwise bending deformations that cannot be represented with this model.

Appendix A

The cross-section integrals of the beam element are defined as

1) Modulus Weighted Section Integrals:

$$EA = \int\int_A Q'_{11}\, d\eta\, d\zeta$$

$$EA_\eta = \int\int_A Q'_{11}\eta\, d\eta\, d\zeta$$

$$EA_\zeta = \int\int_A Q'_{11}\zeta\, d\eta\, d\zeta$$

$$EI_{\eta\eta} = \int\int_A Q'_{11}\zeta^2\, d\eta\, d\zeta$$

$$EI_{\zeta\zeta} = \int\int_A Q'_{11}\eta^2\, d\eta\, d\zeta$$

$$EI_{\eta\zeta} = \int\int_A Q'_{11}\eta\zeta\, d\eta\, d\zeta$$

$$EAC_0 = \iint_A Q'_{11}(\eta^2+\zeta^2)\,d\eta\,d\zeta$$

$$EAC_1 = \iint_A Q'_{11}\eta(\eta^2+\zeta^2)\,d\eta\,d\zeta$$

$$EAC_2 = \iint_A Q'_{11}\zeta(\eta^2+\zeta^2)\,d\eta\,d\zeta$$

$$EAC_3 = \iint_A Q'_{11}(\eta^2+\zeta^2)^2\,d\eta\,d\zeta$$

2) Modulus Weighted Warping Integrals:

$$GJ = \iint_A \left[Q'_{55}(\psi_{,\zeta}+\eta)^2 + Q'_{66}(\psi_{,\eta}-\zeta)^2 + 2Q'_{56}(\psi_{,\eta}-\zeta)(\psi_{,\zeta}+\eta)\right] d\eta\,d\zeta$$

$$EAD_0 = \iint_A Q'_{11}\psi\,d\eta\,d\zeta$$

$$EAD_1 = \iint_A Q'_{11}\psi\eta\,d\eta\,d\zeta$$

$$EAD_2 = \iint_A Q'_{11}\psi\zeta\,d\eta\,d\zeta$$

$$EAD_3 = \iint_A Q'_{11}\psi^2\,d\eta\,d\zeta$$

$$EAD_4 = \iint_A Q'_{11}\psi(\eta^2+\zeta^2)\,d\eta\,d\zeta$$

$$EAD_5 = \iint_A Q'_{11}\psi\psi_{,x}\,d\eta\,d\zeta$$

$$EAD_6 = \iint_A Q'_{11}\psi_{,x}\,d\eta\,d\zeta$$

$$EAD_1' = \iint_A Q'_{11}\psi_{,x}\eta\,d\eta\,d\zeta$$

$$EAD_2' = \iint_A Q'_{11}\psi_{,x}\zeta\,d\eta\,d\zeta$$

$$EAD_3' = \iint_A Q'_{11}\psi_{,x}{}^2\,d\eta\,d\zeta$$

$$EAD_4' = \iint_A Q'_{11}\psi_{,x}(\eta^2+\zeta^2)\,d\eta\,d\zeta$$

3) Anisotropic Material Stiffness Coupling Integrals:

$$EAB_0 = \iint_A \left\{Q'_{15}(\psi_{,\zeta}+\eta) + Q'_{16}(\psi_{,\eta}-\zeta)\right\} d\eta\,d\zeta$$

$$EAB_1 = \iint_A \left\{Q'_{15}(\psi_{,\zeta}+\eta) + Q'_{16}(\psi_{,\eta}-\zeta)\right\}\eta\,d\eta\,d\zeta$$

$$EAB_2 = \iint_A \left\{Q'_{15}(\psi_{,\zeta}+\eta) + Q'_{16}(\psi_{,\eta}-\zeta)\right\}\zeta\,d\eta\,d\zeta$$

$$EAB_3 = \iint_A \left\{Q'_{15}(\psi_{,\zeta}+\eta) + Q'_{16}(\psi_{,\eta}-\zeta)\right\}\psi\,d\eta\,d\zeta$$

$$EAB_3' = \iint_A \left\{Q'_{15}(\psi_{,\zeta}+\eta) + Q'_{16}(\psi_{,\eta}-\zeta)\right\}\psi_{,x}\,d\eta\,d\zeta$$

$$EAB_4 = \iint_A \left\{Q'_{15}(\psi_{,\zeta}+\eta) + Q'_{16}(\psi_{,\eta}-\zeta)\right\}(\eta^2+\zeta^2)\,d\eta\,d\zeta$$

4) Mass Weighted Section Integrals:

$$m = \iint_A \rho\,d\eta\,d\zeta \qquad Im_{\eta\eta} = \iint_A \rho\zeta^2\,d\eta\,d\zeta$$

$$m\eta_m = \iint_A \rho\eta\,d\eta\,d\zeta \qquad Im_{\zeta\zeta} = \iint_A \rho\eta^2\,d\eta\,d\zeta$$

$$m\zeta_m = \iint_A \rho\zeta\,d\eta\,d\zeta \qquad Im_{\eta\zeta} = \iint_A \rho\eta\zeta\,d\eta\,d\zeta$$

Acknowledgments

The authors would like to express their gratitude to the Engineering Mechanics Department and the Engineering Sciences Laboratory, TRW Co., Redondo Beach, California for their support of this research. Thanks to Dr. D. Crawford of TRW for developing a program that generates the blade geometric data and to Oral Mehmed of NASA-Lewis for supplying the experimental results.

References

[1]Whitlow, J. B., Jr. and Sievers, G. K., "Fuel Savings Potential of NASA Advanced Turboprop Program," NASA TM-83736, Sept. 1984.

[2]Brown, K. W., Harvey, P. R., and Chamis, C. C., "Structural Tailoring of Advanced Turboprops," *Proceedings of the 28th AIAA/ASME/ASCE/AHS Structures, Structural Dynamics, and Materials Conference,* Monterey, CA, Vol. 1, 1987, pp. 827-837.

[3]Hodges, D. H. and Dowell, E. H., "Nonlinear Equations of Motion for the Elastic Bending and Torsion of Twisted Nonuniform Rotor Blades," NASA TN-D-7818, Dec. 1974.

[4]Rosen, A. and Friedmann, P. P., "Nonlinear Equations of Equilibrium for Elastic Helicopter or Wind Turbine Blades Undergoing Moderate Deflection," NASA CR-159478, Dec. 1978.

[5]Hodges, D. H., "Nonlinear Equations for Dynamics of Pretwisted Beams Undergoing Small Strains and Large Rotations," NASA TP-2470, May 1985.

[6]Rosen, A., "Theoretical and Experimental Investigation of the Nonlinear Torsion and Extension of Initially Twisted Bars," *ASME Journal of Applied Mechanics,* Vol. 50, June 1983, pp. 321-326.

[7]Hodges, D. H., "Torsion of Pretwisted Beams Due to Axial Loading," *ASME Journal of Applied Mechanics,* Vol. 47, June 1980, pp. 393-397.

[8]Kaza, K. K. and Kielb, R. E., "Effects of Warping and Pretwist on Torsional Vibration of Rotating Beams," *ASME Journal of Applied Mechanics,* Vol. 51, December 1984, pp. 913-920.

[9]Rosen, A. and Rand, O., "Numerical Model of the Nonlinear Behavior of Curved Rods," *Computers and Structures,* Vol. 22, No. 5, 1986, pp. 785-799.

[10]Hong, C. and Chopra, I., "Aeroelastic Stability Analysis of a Composite Rotor Blade," *Journal of the American Helicopter Society,* Vol. 30, No. 2, April 1985, pp. 57-67.

[11]Bauchau, O. A. and Hong, C. H., "Finite Element Approach to Rotor Blade Modeling," *Journal of the American Helicopter Society,* Vol. 32, No. 1, Jan. 1987, pp. 60-67.

[12]Stemple, A. D. and Lee, S. W., "A Finite Element Model for Composite Beams with Arbitrary Cross-Sectional Warping," *Proceedings of the 28th AIAA/ASME/ASCE/AHS Structures, Structural Dynamics, and Materials Conference,* Monterery, CA, Vol. I, 1987, pp. 304-313.

[13]Bauchau, O. A., "A Beam Theory for Anisotropic Materials," *Journal of Applied Mechanics,* Vol. 52, 1985, pp. 416-422.

[14]Mason, W. E. and Hermann, L. R., "Elastic Shear Analysis of General Prismatic Beams," *Journal of Engineering Mechanics Division,* Vol. 94, EM4, Aug. 1968, pp. 965-983.

[15]Wörndle, R., "Calculation of the Cross Section Properties and the Shear Stresses of Composite Rotor Blades," *Vertica,* Vol. 6, 1982, pp. 111-129.

[16]Kosmatka, J. B., "Structural Dynamic Modeling of Advanced Composite Propellers by the Finite Element Method," Ph.D. Dissertation, Univ. of California, Mechanical, Aerospace and Nuclear Engineering Department, Los Angeles, CA, 1986.

[17]Wempner, G., *Mechanics of Solids with Applications to Thin Bodies,* 1st ed., McGraw-Hill, New York, 1973.
[18]Lekhnitskii, S. G., *Theory of Elasticity of an Anisotropic Body,* 1st ed., Holden-Day, San Francisco, 1963.
[19]Gupta, K. K., "Development of a Unified Numerical Procedure for Free Vibration Analysis of Structures," *International Journal of Numerical Methods in Engineering,* Vol. 17, 1981, pp. 187–198.
[20]Glatt, L., Kosmatka, J. B., Crawford, D., and Wong, E., *Generalized Aviation Propeller Analysis System,* NASA Final Report, 1987.
[21]Kosmatka, J. B. and Friedmann, P. P., "Structural Dynamic Modeling of Advanced Composite Propellers by the Finite Element Method," *Proceedings of the 28th AIAA/ASME/ASCE/AHS Structures, Structural Dynamics, and Materials Conference,* Monterey, CA, Vol. II, 1987, pp. 111–124.